Unidirectionally oriented nanocracks on metal surfaces irradiated by low-fluence femtosecond laser pulses

Masahiro Shimizu, Masaki Hashida, Yasuhiro Miyasaka, Shigeki Tokita, and Shuji Sakabe

Citation: Applied Physics Letters **103**, 174106 (2013); doi: 10.1063/1.4827296
View online: http://dx.doi.org/10.1063/1.4827296
View Table of Contents: http://scitation.aip.org/content/aip/journal/apl/103/17?ver=pdfcov
Published by the AIP Publishing

Unidirectionally oriented nanocracks on metal surfaces irradiated by low-fluence femtosecond laser pulses

Masahiro Shimizu,[1,a)] Masaki Hashida,[1,2] Yasuhiro Miyasaka,[1,2] Shigeki Tokita,[1,2,b)] and Shuji Sakabe[1,2]

[1]*Advanced Research Center for Beam Science, Institute for Chemical Research, Kyoto University, Uji, Kyoto 611-0011, Japan*

[2]*Department of Physics, Graduate School of Science, Kyoto University, Kitashirakawa, Sakyo, Kyoto 606-8502, Japan*

(Received 20 August 2013; accepted 14 October 2013; published online 25 October 2013)

We have investigated the origin of nanostructures formed on metals by low-fluence femtosecond laser pulses. Nanoscale cracks oriented perpendicular to the incident laser polarization are induced on tungsten, molybdenum, and copper targets. The number density of the cracks increases with the number of pulses, but crack length plateaus. Electromagnetic field simulation by the finite-difference time-domain method indicates that electric field is locally enhanced along the direction perpendicular to the incident laser polarization around a nanoscale hole on the metal surface. Crack formation originates from the hole. © *2013 AIP Publishing LLC*. [http://dx.doi.org/10.1063/1.4827296]

Nanostructures formed on metals by femtosecond laser irradiation have attracted much interest due to applications such as coloration,[1,2] friction reduction,[3] wettability modification,[4,5] and surface-enhanced Raman scattering.[6] Periodic grating structures in particular have been intensively investigated; their formation is currently attributed to surface plasmons,[7,8] interference between incident light and surface plasmons,[9,10] or interference between incident light and scattered light.[11–13] The grating period depends on laser irradiation parameters such as fluence,[7,8] number of pulses,[14] and laser wavelength (λ_L)[14] and falls between $0.5\lambda_L$ and $0.85\lambda_L$ (Ref. 7) at fluence above the ablation threshold fluence (F_{th}), which can be defined by fitting the laser fluence dependence of ablation rate to $l = \alpha^{-1} \ln(F_L/F_{th})$,[15,16] where l, α, and F_L are ablation rate, optical absorption (or heat penetration coefficient), and laser fluence, respectively. Even at the fluence below F_{th}, a structure with a much shorter interspace ($\sim 0.3\lambda_L$) has been observed in copper after irradiation of many pulses,[7,17] and emission of energetic ions has been observed.[18] The formation process of nanostructures below F_{th} should be different from that above F_{th}, yet no physical interpretation has been put forward for the nanostructure formation in the low fluence range. Understanding the physical process is important for the application mentioned above and for the development of laser nanoprocessing. In this study, we have investigated the morphology and formation mechanism of surface nanostructures on metal targets [tungsten (W), molybdenum (Mo), copper (Cu), platinum (Pt)] irradiated by femtosecond laser pulses below F_{th}. The surface nanostructures observed here have no periodicity, so we cannot apply the formation mechanism for a periodic structure to these surface nanostructures.

We used linearly polarized laser pulses (40 fs pulse duration, 800 nm center wavelength, 10 Hz repetition rate) from a Ti:sapphire chirped-pulse amplification system (ICR, Kyoto University). In air, the laser pulses were focused onto the metal targets by a spherical lens with focal length of 100 mm. To avoid the spatial non-uniformity of laser fluence, a flat-top profile was formed, and the diameter of the flat-top region was 35 μm. The targets were W, Mo, Cu, and Pt metals, which had been mechanically polished. The pulse energy was adjusted by two polarizers and a pair of half-wave plates. For each metal, the incident pulse number was varied with the

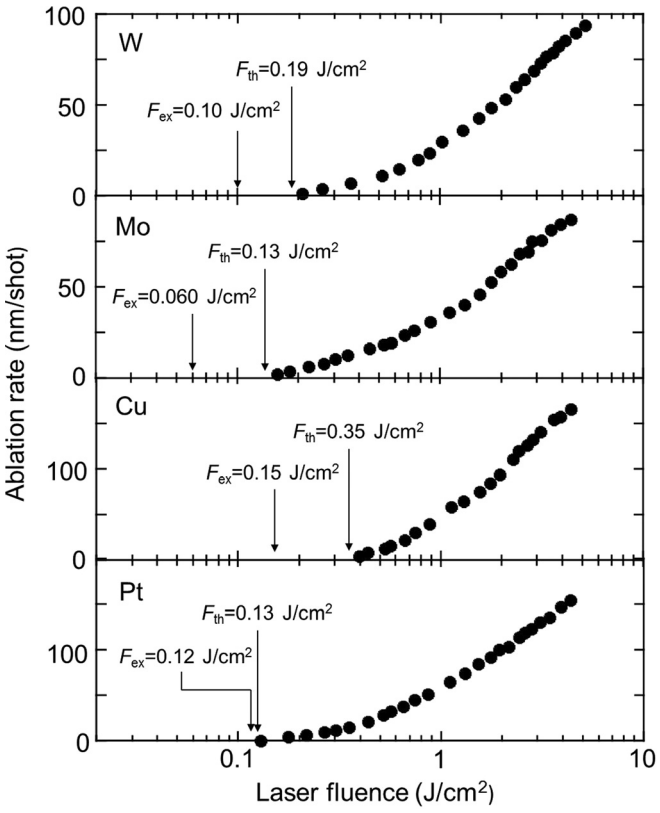

FIG. 1. Laser fluence dependence of ablation rate. Arrows indicate ablation threshold fluences (F_{th}) determined by fitting the laser fluence dependence of ablation rate to $l = \alpha^{-1} \ln(F_L/F_{th})$ and fluences for the present experiment (F_{ex}).

[a)]Author to whom correspondence should be addressed. Electronic mail: m.shimizu@curl1.kuic.kyoto-u.ac.jp. Present address: Department of Material Chemistry, Graduate School of Engineering, Kyoto University, Kyoto 615-8510, Japan.

[b)]Present address: Institute of Laser Engineering, Osaka University, Suita, Osaka 565-0871, Japan.

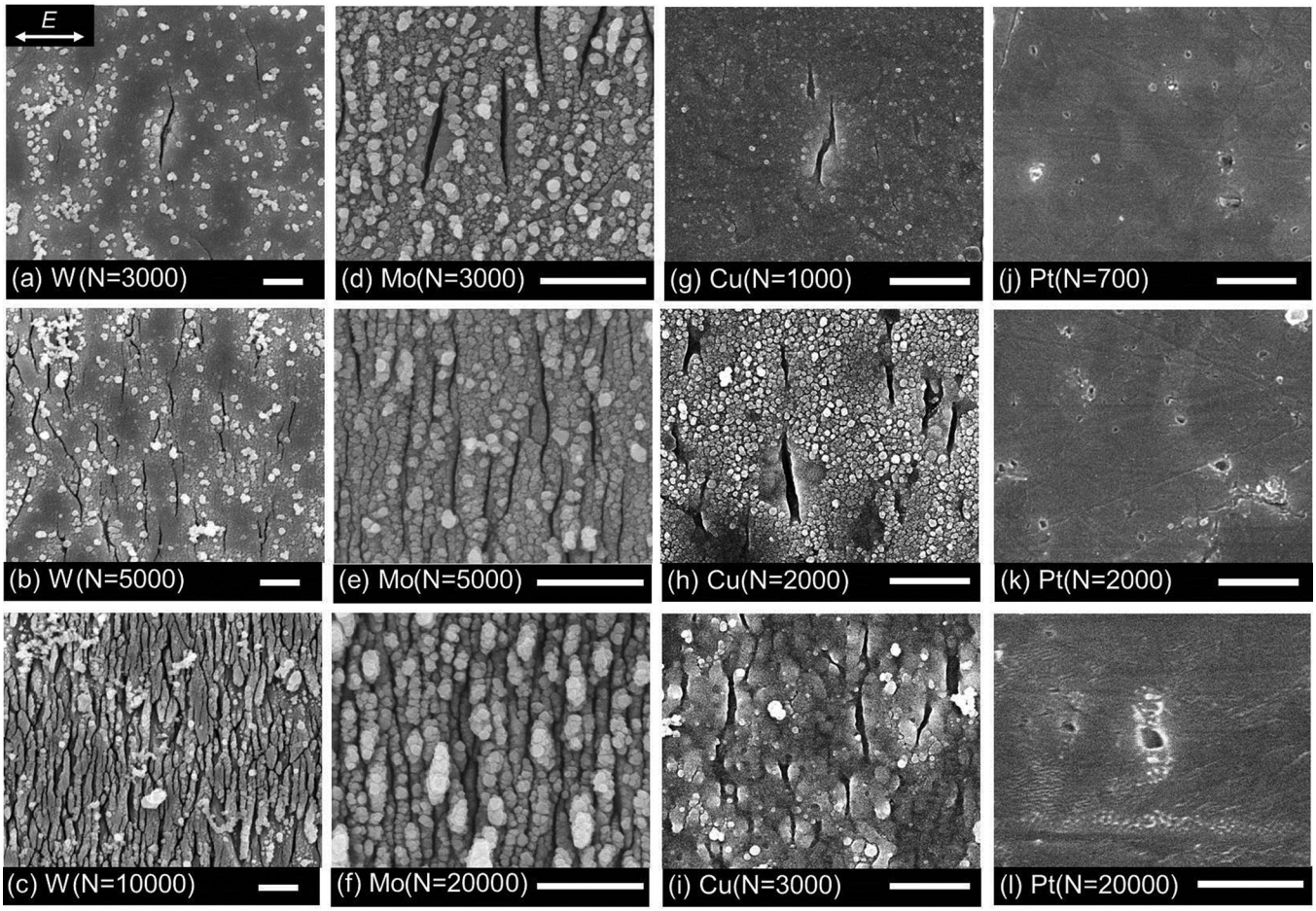

FIG. 2. FESEM images of surface nanostructures on (a)–(c) W, (d)–(f) Mo, (g)–(i) Cu, and (j)–(l) Pt. The double arrow in (a) shows the polarization direction of the incident laser field, which is the same for all images. N is the number of incident pulses. The white bar in each image corresponds to 500 nm.

laser fluence fixed below F_{th}. The ablation threshold fluence is determined by fitting the laser fluence dependence of ablation rate to $l = \alpha^{-1} \ln(F_L/F_{th})$. To evaluate ablation rate, we measured crater depth with a confocal laser scanning microscope (HL-150, Lasertec). Figure 1 shows the laser fluence dependence of ablation rate, the ablation threshold fluence (F_{th}), and fluences for the present experiment (F_{ex}). The irradiated spots were observed by a field-emission scanning electron microscopy (FESEM; JSM-6700F, JEOL).

Figures 2(a)–2(i) show FESEM images of W, Mo, Cu, and Pt surfaces after irradiation of multiple laser pulses. For W, Mo, and Cu, nanocracks oriented perpendicular to the incident laser polarization were generated, and the number density of the cracks increased with the number of incident laser pulses. In this letter, we refer to the aggregation of nanocracks as a "striped structure." The interspaces between the nanocracks on W (10 000 shots) and Mo (20 000 shots) are 50–200 and 50–150 nm, respectively. The number density of nanocracks on Cu (3000 shots) is smaller than that on W and Mo. The minimum interspace of the nanocracks on Cu (3000 shots) is 70 nm. The power spectra obtained by 2D Fourier transform of the images of the striped structures contain no sharp peak, which indicates that the striped structures were not periodic arranged. For Pt, nanocracks were not induced even after 20 000 pulses, but a structural change was observed around hole of 130 nm in diameter along the direction perpendicular to the laser polarization.

Since the diameter of the flat-top region of the laser beam (35 μm) was much larger than the size of a nanocrack ($\sim$1 μm or smaller), the nanocrack formation was not attributed to spatial non-uniformity of incident laser fluence. We hypothesized that the nanoscale roughness on metal surfaces would cause the nanocrack formation. To examine the formation process, we simulated the intensity distribution of electric field around a nanoscale hole (nanohole) on a metal surface by the finite-difference time-domain method.

We used commercially available software (Poynting, Fujitsu). The modeled nanohole is shown in Fig. 3(a). A hemispherical hole of 50 nm in diameter was put in a metal surface. A continuous wave (800 nm wavelength, 1 V/m electric field amplitude) was injected perpendicular to the surface. The complex refractive indices used in the simulation were $3.5 + 2.7i$ (W), $3.6 + 3.3i$ (Mo), $0.24 + 5.0i$ (Cu), and $2.8 + 4.9i$ (Pt).[19] There is a report that complex refractive index does not change during the interaction of a 100 fs laser pulse with a gold surface.[20] The intensity distribution is observed on the metal surface. Figure 3(b) shows the intensity distribution of electric field on the W surface. The electric field was enhanced around the nanohole in the direction perpendicular to the laser polarization and was diminished in the direction parallel to it. The nanocrack direction observed in the present experiment was the same as the direction of electric field enhancement, which we suggest is the cause of the nanocracks observed for W, Mo, and Cu. However,

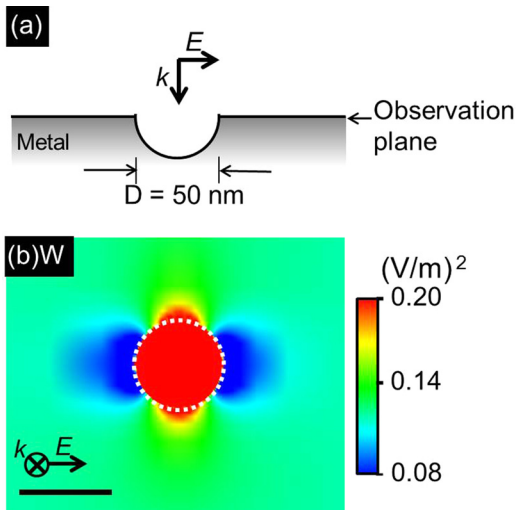

FIG. 3. Electric field intensity around the 50-nm-diameter hole in W calculated by the finite-difference time-domain method. (a) Modeled shape and (b) intensity distributions. The amplitude of incident light is normalized to 1 V/m. The white dotted line indicates the rim of the hole. The black bar corresponds to 50 nm.

nanocracks were not observed on Pt even though a similar enhancement was observed in the simulation. We propose the following mechanism for the crack formation. (1) A fs laser pulse is absorbed, and the temperature rapidly increases and then decreases on the metal surface. (2) Thermal stress due to the heating and cooling induces a tiny crack on the metal surface.[21] (3) When the next pulse comes, the electric field is enhanced around the tiny crack in the direction perpendicular to the laser polarization, thus inducing intense thermal stress in the enhanced field region and producing a nanocrack. (4) Subsequent laser pulses extend the nanocrack. Although we cannot confidently explain why no cracks form on platinum, a possible reason is its high ductility.[22]

Figure 4 shows the histogram of crack length after 5000 and 3000 pulses for W. The crack length at the frequency peak for 5000 pulses was equal to that for 3000 pulses. The maximum length was less than 1.5 μm in both cases. As the number of pulses increased, the crack length distribution did not shift to longer lengths and only the number density of crack increased. To understand this trend, we simulated the enhancement factor of the electric field at the crack edge for W metal. We modeled the nanocrack as a hemi-ellipsoidal hole [Fig. 4(b), inset], with the semi-major axis perpendicular to the laser polarization, and we calculated the hole-length (L) dependence of the field enhancement factor at two positions, namely, at the semi-major axis and at the semi-minor axis along the hold edge. The intensities at these points are I_{long} and I_{short}, respectively. The enhancement factor (η) is defined as I/I_{far}, where I_{far} is the intensity at a position very far from the hole. For I_{long}, the value of η reaches a maximum around $L = 200$ nm and then decreases with increasing L. This indicates that crack extension is limited. The enhancement factor for a deep hole is larger than that for a shallow hole. Therefore, in our experiment, the variance in the crack length distribution was due to the variation of depth, width, and length of the initial tiny crack. These features will depend on the initial surface state of the metal targets and laser irradiation parameters such as fluence and

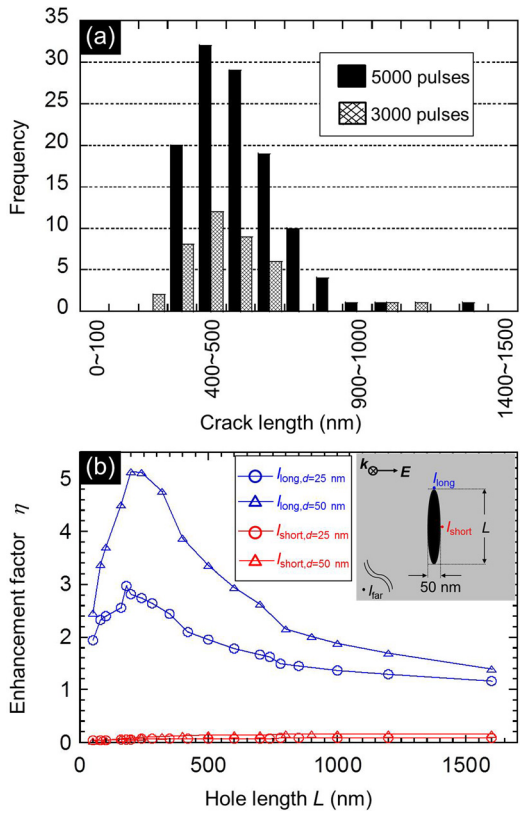

FIG. 4. (a) Histograms of crack length after 5000- and 3000-pulse irradiations (measured and counted in a 12 μm × 9.6 μm area of each FESEM image). In counting, we eliminated cracks that had interconnections or branching. (b) Hole length dependence of electric field enhancement factor for W. The inset shows the modeled shape and the observation points of intensity. The enhancement factor is calculated by the ratio of intensity at the edge to that at a position very far from the hole. The hole is hemi-ellipsoidal. The parameter d is depth at the center.

incident pulse number. In the experiment, only the number of incident laser pulse was different (5000 and 3000 pulses). If the features of initial cracks are independent on the incident pulse number, the crack length distribution will be independent on the number of laser pulses.

Near the hole edge at the semi-minor axis, the field is almost zero. As shown in Fig. 3(b), the low intensity field spans several tens nanometers. In this region, further modification such as additional formation of new tiny cracks will not be induced. The width of this low field region in the laser polarization direction would determine only the minimum interspaces of the striped structures. Therefore, the striped structures do not have periodicity. This is clearly different from the case above F_{th}, in which the surface structure has periodicity derived from surface plasmons or scattered light.[7–13]

In summary, we have observed the generation of nanocracks oriented perpendicular to the incident laser polarization at fluence below F_{th} for W, Mo, and Cu metal targets. The number density of nanocracks increased with incident pulse number, but their length distributions were independent of it. From the experimental and simulation results, we proposed that an initial tiny crack on the metal surface grows to a nanocrack through local field enhancement. The enhanced field near the hole edge in longitudinal direction of the nanocrack makes the crack longer, and the low intensity field near the edge on short direction governs the space to the next crack.

The authors thank K. Hirao and M. Nishi for assistance with FESEM. The authors also thank T. Kanaya and K. Nishida for assistance with confocal laser scanning microscopy. M. Shimizu is supported by the Research Fellowship for Young Scientists of Japan Society for the Promotion of Science. This research was financially supported by JSPS KAKENHI Grant No. 22560720 and by the Amada Foundation Grant No. AF-2012211.

[1]A. Y. Vorobyev and C. Guo, Phys. Rev. B **72**, 195422 (2005).
[2]A. Y. Vorobyev and C. Guo, Appl. Phys. Lett. **92**, 041914 (2008).
[3]T. Kato and N. Abe, Rev. Laser Eng. **37**, 510–514 (2009).
[4]B. Wu, M. Zhou, J. Li, X. Ye, G. Li, and L. Cai, Appl. Surf. Sci. **256**, 61–66 (2009).
[5]A. Kietzig, S. G. Hatzikiriakos, and P. Englezos, Langmuir **25**, 4821–4827 (2009).
[6]C. Wang, Y. Chang, J. Yao, C. Luo, S. Yin, P. Ruffin, C. Brantley, and E. Edwards, Appl. Phys. Lett. **100**, 023107 (2012).
[7]S. Sakabe, M. Hashida, S. Tokita, S. Namba, and K. Okamuro, Phys. Rev. B **79**, 033409 (2009).
[8]K. Okamuro, M. Hashida, Y. Miyasaka, Y. Ikuta, S. Tokita, and S. Sakabe, Phys. Rev. B **82**, 165417 (2010).
[9]M. Huang, F. Zhao, Y. Cheng, N. Xu, and Z. Xu, ACS Nano **3**, 4062–4070 (2009).
[10]G. Obara, N. Maeda, T. Miyanishi, M. Terakawa, N. N. Nedyalkov, and M. Obara, Opt. Express **19**, 19093–19103 (2011).
[11]J. E. Sipe, J. F. Young, J. S. Preston, and H. M. van Driel, Phys. Rev. B **27**, 1141–1154 (1983).
[12]J. F. Young, J. S. Preston, H. M. van Driel, and J. E. Sipe, Phys. Rev. B **27**, 1155–1172 (1983).
[13]J. F. Young, J. E. Sipe, and H. M. van Driel, Phys. Rev. B **30**, 2001–2015 (1984).
[14]A. Y. Vorobyev and C. Guo, J. Appl. Phys. **104**, 063523 (2008).
[15]B. N. Chichkov, C. Momma, S. Nolte, F. von Alvensleben, and A. Tünnermann, Appl. Phys. A **63**, 109–115 (1996).
[16]S. Preuss, A. Demchuk, and M. Stuke, Appl. Phys. A **61**, 33–37 (1995).
[17]M. Hashida, M. Fujita, M. Tsukamoto, A. F. Semerok, O. Gobert, G. Petite, Y. Izawa, and J.-F. Wagner, Proc. SPIE **4830**, 452–457 (2003).
[18]Y. Miyasaka, M. Hashida, Y. Ikuta, K. Otani, S. Tokita, and S. Sakabe, Phys. Rev. B **86**, 075431 (2012).
[19]E. D. Palik, *Handbook of Optical Constants of Solids* (Academic Press, Washington, DC, 1985).
[20]H. Yoneda, H. Morikami, K. Ueda, and R. M. More, Phys. Rev. Lett. **91**, 075004 (2003).
[21]S. Pestchanyi, I. Garkusha, and I. Landman, Fusion Eng. Des. **85**, 1697–1701 (2010).
[22]S. L. Bazhenov, A. L. Volynskii, V. M. Alexandrov, and N. F. Bakeev, J. Polym. Sci., Part B: Polym. Phys. **40**, 10–18 (2002).